JOURNAL OF PROPULSION AND POWER
Vol. 18, No. 1, January–February 2002

Experimental and Analytical Design Verification of the Dual-Bell Concept

Gerald Hagemann,* Michael Terhardt,† and Dietrich Haeseler‡
Astrium GmbH, 81663 Munich, Germany
and
Manuel Frey§
DLR, German Aerospace Research Center, 74239 Lampoldshausen, Germany

The dual-bell nozzle concept has been investigated analytically and experimentally. Based on earlier analytical and numerical work published by the authors, different dual-bell nozzles were designed and experimentally tested to explore this concept regarding its aerodynamic characteristics. This experimental work included cold-gas and hot-gas subscale tests, which were performed within a joint German/Russian research program TEHORA, complementary to the German national technology program TEKAN. It is shown that, depending on the type of nozzle contour used for the dual-bell nozzle extension, a sudden transition from sea level to altitude mode operation can be achieved. Furthermore, important information from the hot-gas tests regarding the wall heat transfer was gained.

Nomenclature

A	=	area
H	=	flight altitude
I	=	specific impulse
l	=	length
p	=	pressure
q	=	wall heat flux
x	=	axial length
ε	=	area ratio, A/A_{throat}

Subscripts

a	=	ambient
c	=	combustion chamber
e	=	exit
SL	=	side load
sp	=	specific
w	=	wall

Introduction

THE dual-bell nozzle concept, first proposed by Foster and Cowles in 1949,[1] has recently gained renewed interest in the United States,[2,3] Japan,[4] Europe,[5–8] and Russia.[9] The reason for this interest is the unique feature of an one-step altitude adaptation, achieved only by a wall inflection and, thus, without any moving parts. Because of the classical bell-shaped form, necessary changes on the launcher level are small when compared to other altitude adaptive nozzle concepts, for example, plug nozzles.

At low altitudes, controlled and symmetrical flow separation occurs at this wall inflection (see Fig. 1a), which results in a smaller effective area ratio without generating dangerous side loads. At higher altitudes, the nozzle flow is attached to the wall until the exit plane, and the full area ratio is used (see Fig. 1b). Because of the higher area ratio, an increase in vacuum performance is achieved.

The first published experiments on dual-bell nozzles were performed by Horn and Fisher.[2] Their cold-flow subscale nozzle tests proved the altitude adaptive capability of this nozzle concept, but also showed that additional losses are induced compared to a conventional bell-shaped design. A recalculation of the experiments from Ref. 2 were presented by Goel and Jensen.[3] In 1997, Frey and Hagemann presented results of analytical and numerical studies.[6] The dependence of additional losses induced in dual-bell nozzles as a function of nozzle design parameters was systematically investigated, and performance characteristics were compared to a conventional reference bell nozzle. It was shown that additional losses induced by the wall inflection depend on the overall contour design and can be surprisingly low.

Figure 2 shows the dual-bell performance characteristic vs flight altitude. At sea-level operation, the pressure within the separated flow region of the dual-bell nozzle extension is slightly below the ambient pressure, inducing a thrust loss called aspiration drag. In addition, the flow transition from sea-level mode to altitude mode occurs before the optimum crossover point, which leads to a thrust loss compared to an ideal switchover. The nonoptimum contour of the full-flowing dual-bell nozzle in the altitude mode results in further losses.

This paper is a logical continuation of the work presented in Ref. 6. In the next part, results of a combined engine system and trajectory analysis are presented, demonstrating the positive performance impact of a dual-bell nozzle on payload. Then design considerations are discussed. Results of experiments are presented, proving the validity of the design considerations.

Launcher System Study

A launcher system study has been performed within the European FESTIP (Future European Space Transportation Investigation Program) technology study. To compare the dual-bell nozzle concept with a conventional bell nozzle in terms of payload, the launcher concept No. 1 (#1) of the FESTIP system study has been used.[5] This single stage to orbit launcher is a vertical takeoff and horizontal landing vehicle for a payload of 2000 kg in a polar orbit. It uses four booster and four sustainer engines, each designed as fuel-rich staged combustion cycle with equal combustion chambers, but different area ratios for the conventional-bell nozzle design. The booster engines are switched off during ascent, and the sustainer engines are used for the whole ascent. In this study, the nozzles of the sustainer engines are replaced by dual-bell nozzles. The following design

Received 19 August 2000; revision received 4 May 2001; accepted for publication 22 May 2001.

*Engineer, Project Manager, Space Infrastructure Division; gerald.hagemann@astrium-space.com. Member AIAA.
†Engineer, Project Manager, Space Infrastructure Division; michael.terhardt@astrium-space.com. Member AIAA.
‡Engineer, Project Manager, Space Infrastructure Division; dietrich.haeseler@astrium-space.com. Member AIAA.
§Engineer, Space Propulsion; manuel.frey@dlr.de.

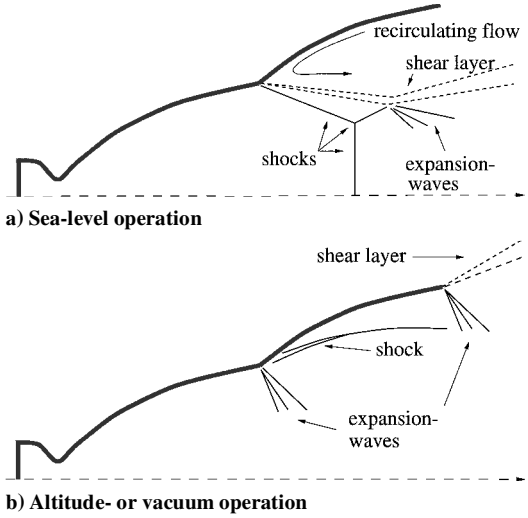

Fig. 1 Different flow regimes in dual-bell nozzles: a) sea-level operation with flow separation at wall inflection and b) altitude mode with full-flowing nozzle.

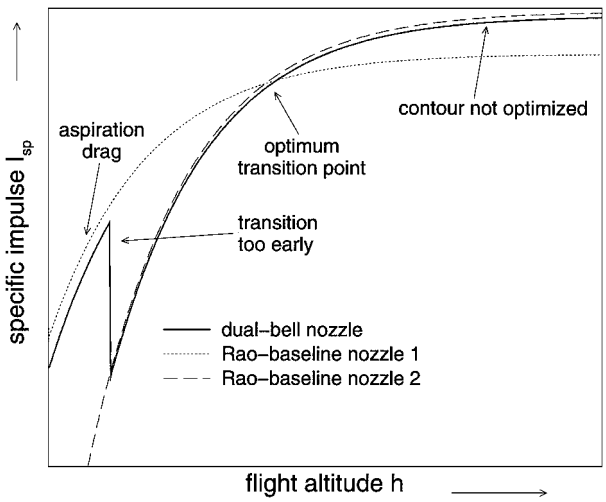

Fig. 2 Performance characteristic of a dual-bell nozzle and two baseline nozzles as function of flight altitude (baseline nozzle 1: same area ratio as dual-bell base nozzle, baseline nozzle 2: same area ratio as nozzle extension).

criteria have been used: no flow separation in the base nozzle at sea level, no flow separation in the extension after transition from sea level to altitude mode, and sea-level thrust assumed to be the same as for the reference configuration. Different dual-bell nozzle contours were optimized with equal area ratios for the base nozzle and extension and the same total length but varying length of the base nozzle ($l_{15\,\mathrm{deg}} = 55$, 65, 75, and 85%) (see Ref. 5 for further details).

The payload increase was calculated for the different dual-bell configurations with the ALTOS code. The remarkable payload gain of the optimum dual-bell launcher configuration is 72% compared with the reference launcher configuration. The main performance data for the optimum dual-bell nozzle configuration are summarized in Table 1. This analysis has impressively demonstrated the positive payload gain achieved by a dual-bell nozzle concept.

The main uncertainty of dual-bell nozzles regarding the aerodynamic behavior during the launcher ascent is the transition of the separation point from the wall inflection to the nozzle exit. Key areas to be explored are pressure ratio at instant of transition, depending on design of wall inflection and nozzle extension; time needed for transition; separation characteristic after transition; side loads generated due to transition; and heat loads on nozzle extension before, during, and after transition. These issues have been addressed in a cold- and hot-gas subscale nozzle test program, and results are presented in the following sections.

Table 1 Performance data for the reference and optimum dual-bell nozzle configuration

	Nozzle type	
Parameters	Dual-bell	Reference configuration
Area ratio of base nozzle	48	——
Area ratio, nozzle extension	115	65.8
Length $l_{15\%}$ of base nozzle	75%	——
Sea-level specific impulse, m/s	3370	3384
Vacuum specific impulse, m/s	4444	4390
Effective payload gain, kg	+1446	Reference

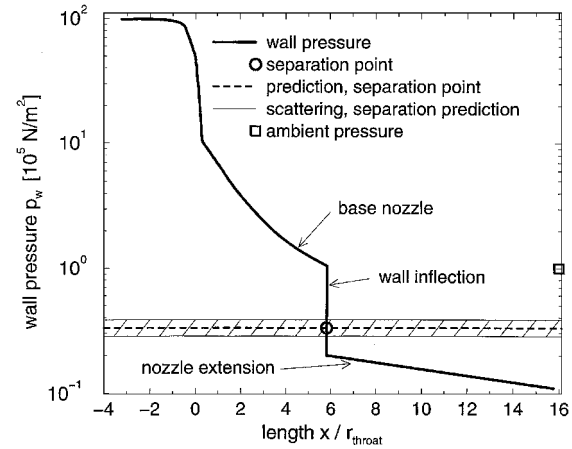

Fig. 3 Wall pressure profile for expansion into vacuum; dual-bell nozzle extension with negative wall pressure gradient. Application of separation criterion at 1-bar ambient pressure, flow separation at $x/r_t = 5.9$.

Design Aspects of Dual-Bell Nozzles

Principle design considerations for dual-bell nozzles have been discussed in detail in Ref. 6. In the following subsections, a brief summary is given.

Inner Contour, Base Nozzle

The inner contour part of dual-bell nozzles, also named the base nozzle, may be designed as a Rao-type bell nozzle for maximum performance or as a truncated ideal nozzle.

Recent investigations performed in Europe within the frame of the flow separation control device program have shown that parabolic or thrust-optimized nozzles feature a specific plume pattern, the cap-shock pattern.[10–14] This plume pattern may trigger a transition from free to restricted shock separation (see Refs. 10 and 11 for a detailed description of this topic). This potential occurrence of restricted shock separation in the base nozzle of a dual-bell nozzle has to be taken into account within the design process.

Wall Inflection and Nozzle Extension

The wall pressure profile of a dual-bell nozzle within the base nozzle is equivalent to that of conventional bell nozzles. At the wall inflection, an expansion fan accelerates the flow. To ensure controlled flow separation at the wall inflection within a certain range of ambient pressures, the required wall pressure value behind the wall inflection is estimated with commonly used separation criteria.[6] The corresponding wall inflection angle is calculated using the well-known Prandtl–Meyer equations.

In a graph showing wall pressure vs nozzle length, as shown in Fig. 3 for a dual-bell nozzle configuration described in detail in Ref. 6, the predicted separation pressure $p_{w,\mathrm{sep}}$ is introduced as a limiting line (or bar, accounting for common uncertainties in exact prediction). The nozzle part with wall pressure values above the line is full flowing, whereas the region with pressure values below is fully separated. During the sea-level mode, the pressure limit given by the line of the separation criterion must, therefore, intersect the wall

pressure profile within the pressure drop at the wall inflection, as shown in Fig. 3. This controlled flow separation at the wall inflection prevents the generation of dangerous side loads commonly observed in conventional overexpanded nozzles featuring uncontrolled flow separation.

Ambient pressure continuously decreases during the ascent of the rocket. In the wall pressure graph shown in Fig. 3, this is linked to a decrease of the separation pressure and, thus, to a movement of the separation line toward lower pressures. At a certain ambient pressure, the bar of the separation criterion intersects the wall pressure profile in the nozzle extension. Different designs of this extension, producing a negative, a zero, or even a positive wall pressure gradient, will lead to different flow behavior.

1) Nozzle extension with negative (or favorable) wall pressure gradient leads to an uncontrolled flow separation within the nozzle extension, as can be observed in conventional conical or bell-shaped nozzles.

2) Within a nozzle extension with zero wall pressure gradient (constant pressure extension), the horizontal bar characterizing the predicted flow separation point reaches all points of the nozzle wall at the same time. This might lead, at least theoretically, to a quick change from sea-level mode to altitude mode. However, in principle, strong nonsymmetric separation, or even a pulsation of the separation point, could be expected from a theoretical point of view.

3) For nozzle extension with positive (or adverse) wall pressure gradient (overturned extension), the predicted separation point intersects the wall pressure profile first in the exit plane of the nozzle, but the full flowing of the nozzle extension first occurs at ambient pressures, where the bar reaches the lowest wall pressure at the wall inflection. Therefore, this type of nozzle extension also might lead, at least theoretically, to a quick change from sea-level mode to altitude mode.

Cold-Gas Tests for Design Verification

Contour Definition for Subscale Nozzles

For the experimental verification of the aforementioned design considerations for dual-bell nozzles, five different nozzle contours were designed and tested. Among these five contours, three different base contours were designed, one truncated ideal base nozzle and two different parabolic base nozzles. The objective for the design of the parabolic base nozzles was to achieve in the first parabolic base a transition from a cap-shock pattern to the classical Mach disk while the separation point is fixed at the wall inflection. Thus, restricted shock separation is unlikely to occur when the separation point features the dual-bell flow transition. The second parabolic base nozzle was designed in such a way that the cap-shock pattern was preserved even for pressure ratios higher than needed for full-flowing of the nozzle extension [this transition from cap-shock pattern to Mach disk and vice versa depends on the axial coordinate, where the internal shock meets the centerline (see Refs. 10 and 11 for a detailed discussion)].

With the truncated ideal base nozzle, the following types of nozzle extension were designed: truncated ideal base nozzle and nozzle extension with favorable wall pressure gradient TICNP, truncated ideal base nozzle and a nozzle extension with zero wall pressure gradient TICCP, and truncated ideal base nozzle and a nozzle extension with positive wall pressure gradient TICPP.

For the two parabolic base nozzles, the following zero wall pressure gradient extensions were designed for testing: parabolic base nozzle 1 with internal shock merging the centerline within nozzle extension PAR1CP and parabolic base nozzle 2 with internal shock position merging the centerline far outside the nozzle extension PAR2CP.

The overall design parameters were kept constant for all dual-bell nozzles and are summarized in Table 2. An inverse design approach was developed and applied for the definition of the nozzle extension contours: The wall pressure profile was prescribed, and the method of characteristics was used to define an appropriate contour. The calculation with the method of characteristics started from the exit plane data for the base nozzle. The latter were extracted from a Two-

Table 2 Dual-bell nozzle design criteria (cold-gas)

Design criterion	Value
Driving gas	Nitrogen
Pressure ratio for full-flowing of base nozzle	$p_c/p_a > 50$
Pressure ratio for fixed separation at wall inflection	$50 < p_c/p_a < 100$
Pressure ratio for full-flowing of nozzle extension	$p_c/p_a > 200$
Area ratio of base nozzle	$\varepsilon \sim 16$
Area ratios of nozzle extensions	$\varepsilon = 36$–45
Nozzle throat radius	$r_{\text{throat}} = 10$ mm
Length of dual-bell nozzle	$x/r_{\text{throat}} = 17$

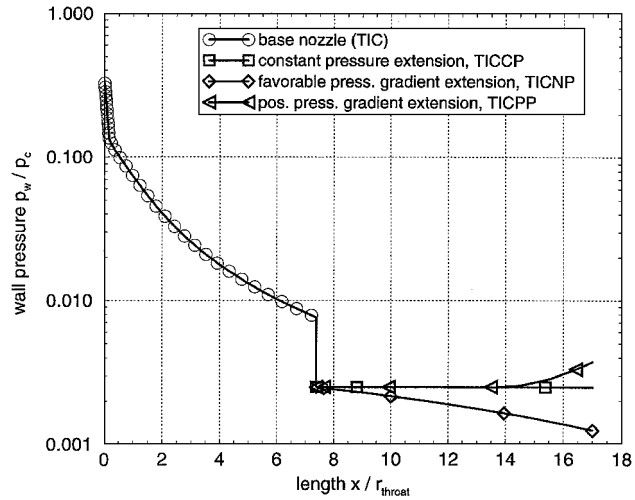

Fig. 4 Prescribed wall pressure profile for cold-gas dual-bell nozzles.

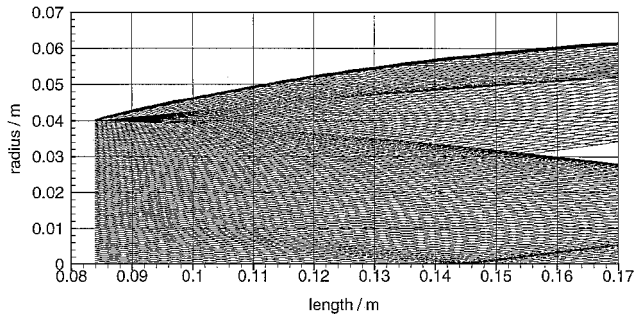

Fig. 5 Mesh generated by method of characteristics within the design process for the constant pressure extension of the PAR1CP nozzle.

Dimensional Kinetics Computer Program (TDK) TDK-flowfield analysis.[15] Figure 4 shows the prescribed wall pressure profiles of the TICNP, TICCP, and TICCP dual-bell nozzles. Figure 5 shows the mesh generated by left- and right- running characteristics, exemplarily shown for the constant pressure extension of the dual-bell PAR1CP. Note that the profile of the internal shock emanating from the base nozzle becomes visible by converging characteristics; the shock is reflected at the centreline at $x \sim 14.5$ cm downstream of the throat.

Before manufacturing and testing, the defined dual-bell nozzles were recalculated with a Navier–Stokes solver. Details of the numerical scheme including validation calculations, as well as for dual-bell nozzles, are presented in Ref. 16. To illustrate the flowfield development for the vacuum condition, Fig. 6 shows Mach number isolines in three different configurations, the TICCP (Fig. 6a), the PAR1CP (Fig. 6b), and the PAR2CP (Fig. 6c). For both dual-bell nozzles with parabolic base nozzles, the difference in internal shock positions becomes visible. For the PAR1CP, the trace of the internal shock predicted by the numerical scheme agrees well with the result of the extension design calculation based on the method of characteristics (see Figs. 5 and 6). Besides the internal shock in both parabolic base nozzles, further shock formation can be observed in all three nozzle

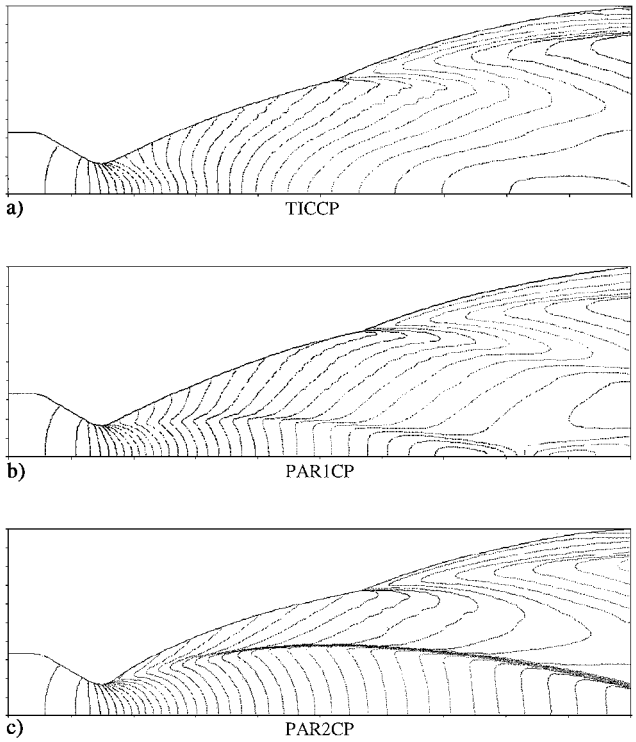

Fig. 6 Mach number isolines in three dual-bell configurations, $\Delta M = 0.1$.

extensions shown in Fig. 6: This shock is induced directly behind the wall inflection, and it compresses the expanding core flow to the desired wall pressure. (Figure 1b also shows this shock near the wall in the dual-bell nozzle extension.) The shock strength depends on the wall pressure profile prescribed within the nozzle design. Consequently, the shock is also observed in the dual-bell contour design calculation for the nozzle extension (see Fig. 5). For example, for the PAR1CP, the compression shock leaves the exit plane of the mesh generated by left- and right-running characteristics at a radius of $r \sim 0.05$ m (see Figs. 5 and 6).

The comparison of prescribed and recalculated wall pressure profiles shows perfect agreement, thereby proving and validating the correct design approach. The comparison for the TICPP and TICNP dual-bell nozzle will be discussed subsequently, together with experimental pressure data.

Cold-Gas Subscale Dual-Bell Test Campaign

The five different dual-bell nozzles were tested in the P6.2 nozzle test facility at DLR, German Aerospace Research Center, Lampoldshausen. This test facility uses the self-sustained diffuser principle to establish a near vacuum with a lowest pressure of $p_a \sim 0.2$ bar in the altitude chamber. In Ref. 12 further details are given on the test facility and typical setups for subscale nozzle test campaigns.

Pure gaseous nitrogen was used as the driving fluid to avoid condensation effects. High-frequency pressure transducers were installed in different axial and circumferential positions. Kulite XT-154-190M-1-bar-A absolute pressure transducers were used with a measurement accuracy of 1 mbar. Before each test campaign, all transducers were calibrated for absolute pressure values with a parabolic transfer function. Before each test run, each transducer measuring chain was corrected for the zero offset against a high-accuracy ambient pressure barometer, the latter with an accuracy of 0.1 mbar. Strain gauges and vibration measurements were also recorded during each test campaign. Further information, especially on the calibration of measurement transducers is given in Ref. 12.

A typical test sequence consists of several chamber pressure ramps from $p_c = 1$ bar up to $p_c = 50$ bar, corresponding to pressure ratios of $p_c/p_a = 1$ up to $\sim$300. Thus, achievable pressure ratios are sufficient to meet the chosen design pressure ratios for the

Fig. 7 Color schlieren image of TICCP plume flow in P6.2: top, TICCP in near vacuum operation, with incipient flow separation near nozzle exit, Mach disk in plume (not visible) and bottom, TICCP in sea-level operation, with controlled flow separation at wall inflection, Mach disk in plume is visible.

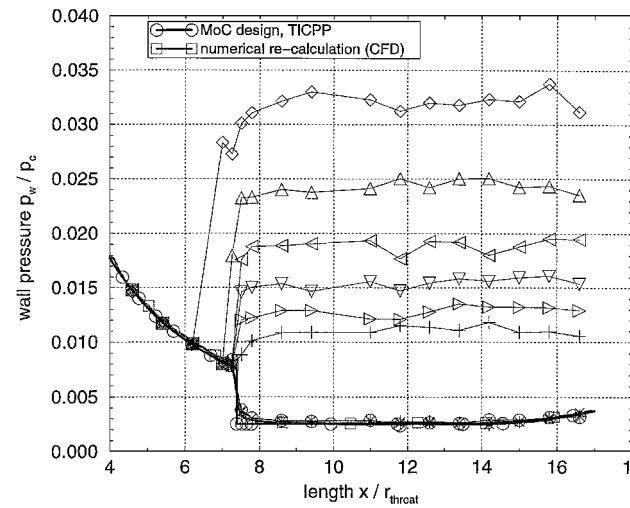

Fig. 8 Wall pressures measured during upramping of chamber pressures p_c/p_a in TICPP.

dual-bell nozzles. The ramping speed was thereby varied between $\partial(p_c/p_a)/\partial t \approx 0{,}5$–2/s.

Test results are briefly discussed, exemplary only for the truncated ideal contour-based dual-bell configurations. Figure 6 shows the TICCP-nozzle hardware mounted inside the P6.2 altitude chamber, with opened windows. Figure 7 shows color schlieren images exposed during a test sequence with the TICCP in both operation modes, sea-level and near-vacuum operation.

Wall pressure data p_w/p_a instantaneously measured in the TICPP at different chamber pressure ratios p_c/p_a at an upramping of chamber pressure ratio are shown in Fig. 8. Pressure data are shown for $30 < p_c/p_a < 110$, $\Delta p_c/p_a = 10$ [high frequency (HF) pressure measurement are instantaneously measured at pressure ratios during transient ramping]. At a chamber pressure ratio of

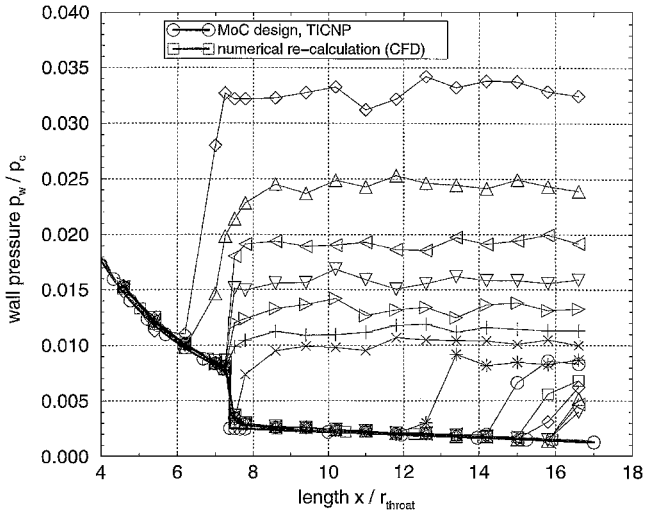

Fig. 9 Wall pressures measured during upramping of chamber pressures p_c/p_a in TICNP.

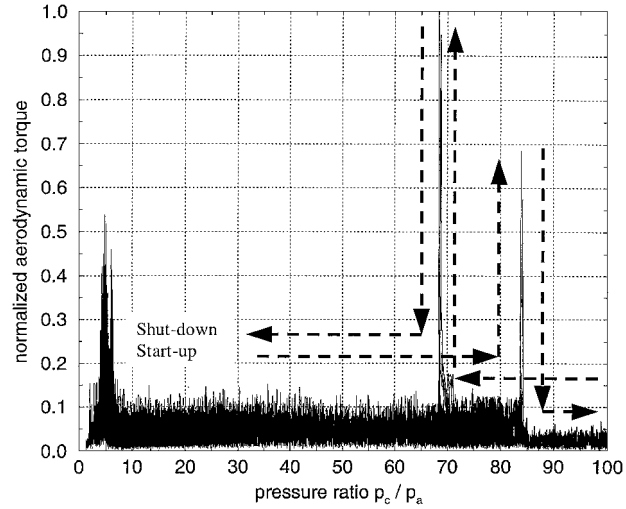

Fig. 10 Normalized aerodynamic side-load torque measured during two pressure ratio p_c/p_a ramps for the TICPP-nozzle; maximum side-load torque used for normalization.

$(p_c/p_a)_{\text{trans, st-up}} \approx 85$, a sudden transition of the separation point from the wall inflection to the nozzle exit was recorded, which lasts less than 10 ms. In repetitive tests with different pressure ramps, this sudden transition occurred always at the same pressure ratio $(p_c/p_a)_{\text{trans, st-up}}$. During downramping of the chamber pressure ratio, and thus simulating a shut-down sequence, a significant hysteresis in pressure ratio p_c/p_a at the instant of transition was observed, with a much lower transition pressure ratio $(p_c/p_a)_{\text{trans, sh-dw}}$ during shut down. The TICCP nozzle featured a similar separation characteristic. The observed hysteresis supports the dual-bell concept because a pulsation in the transitional pressure ratio range during start up or shut down is unlikely to occur.

The measured timescales needed for transition in the positive pressure gradient and constant pressure extensions are much lower compared to the timescales gained from theoretical considerations as published in Ref. 6.

At the wall inflection of the TICNP, stable and controlled flow separation was also observed until $(p_c/p_a)_{\text{trans, st-up}}$. However, for higher pressure ratios, the TICNP nozzle featured a more regular separation characteristic with stable but uncontrolled flow separation in the extension, until full flowing was achieved. Figure 9 shows details of the wall pressure measurements. Pressure data are shown for $30 < p_c/p_a < 160, \Delta p_c/p_a = 10$ (HF pressure measurements are instantaneously measured at given pressure ratios during transient ramping).

The transition pressure ratio in the dual-bell nozzles during simulated start up occurred in the experiments slightly earlier than assumed within the design phase (see Table 2). The reasons for this are that the aspiration drag in the nozzle extension is not taken into account within the design and there are common uncertainties inherently connected with any separation prediction model.

Figure 10 shows a typical side-load characteristic of a dual-bell nozzle featuring a sudden transition, exemplarily shown for the TICPP. Figure 10 includes the side-load information during both upramping and downramping of the chamber pressure ratio p_c/p_a from several pressure ramps. The transition from sea-level to vacuum operation during start up or upramping of chamber pressure ratio p_c/p_a induces the distinct side-load peak at $(p_c/p_a)_{\text{trans,st-up}} \approx 85$. For higher pressure ratios, full flowing in the dual-bell nozzle is achieved. The second peak observed close to $p_c/p_a \approx 70$ is caused by the transition from vacuum to sea-level operation during downramping of the pressure ratio p_c/p_a. This means, that during shut down, the vacuum flowfield condition is preserved within the nozzle down to $(p_c/p_a)_{\text{trans,sh-dw}} \approx 70$.

The observed side-load peaks at very low pressure ratios of $p_c/p_a \approx 5$ are induced by an inherent instability of the supersonic exhaust jet (see Ref. 12 for a detailed analysis) and are the subject of further investigation.

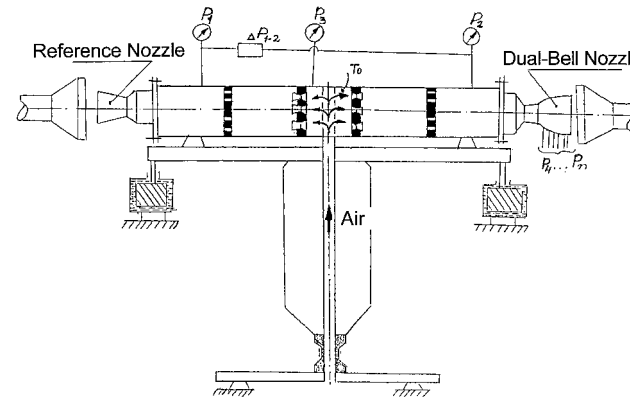

Fig. 11 Schematic of nozzle test bench at Keldysh Research Center, Moscow.

Hot-Versus Cold-Gas Dual-Bell Tests

In addition to the cold-gas dual-bell tests performed, complementary tests with cold- and hot-gas were planned and performed in a cooperation with Astrium; DLR, German Aerospace Research Center; and the Chemical Automatics Design Bureau in Voronezh, Russia. These dual-bell tests were performed at the Keldysh Research Center in Moscow. Figure 11 shows the test bench used for the nozzle tests. Air supplied from storage tanks enters the test bench from below at a pressure of approximately 200 bar at room temperature. The airflow is then distributed equally to the left and right side by sonic nozzles. The dual-bell nozzle is attached at one side, whereas a reference nozzle at the other side is used for thrust tests only.

Hot air at a temperature of about 1000 K is generated by the burning of alcohol. The combustion itself takes place outside the main flow path; the combustion products are injected into the main airflow at the second orifice plate.

To study the influence of the main nozzle design parameters, an extensive flow test program was conducted. In a first step, several subscale nozzle models were tested with air at room temperature allowing a systematic variation of the area ratio, contour turn angle at the inflection point, and nozzle exit angle. In these flow tests, the static pressure profile along the wall and the thrust were measured. One specific dual-bell contour was then chosen for further cold- and hot-gas tests, the results of which are given in the following paragraphs.

Dual-bell nozzle design parameters are included in Table 3. The maximum area ratios realized in this test campaign are significantly lower than compared to the cold-gas design data included in Table 2.

Table 3 Dual-bell nozzle design parameter (hot- vs cold-gas test campaign within Program on Technologies for Components of High Performance Rocket Engines, TEHORA)

Design criterion	Value
Driving gas	Ambient air, and air plus alcohol
Area ratio of base nozzle	$\varepsilon = 2.8$
Area ratios of nozzle extensions	$\varepsilon = 8.1$
Nozzle throat radius	$r_{\text{throat}} = 18$ mm

Fig. 12 Temperature sensors mounted to nozzle model for hot-gas tests.

The reason for this significant reduction was to avoid any condensation effects in cold-flow tests because the one-dimensional nozzle exit Mach number was limited to 3.7. The inner base nozzle part was designed as a truncated ideal base nozzle. For the hot-gas tests, a negative pressure gradient contour was chosen for the nozzle extension.

The transient wall temperature was measured by 16 temperature sensors attached to the outside in a sector where the nozzle wall was thinned to approximately 1 mm (see Fig. 12). The measurements were recorded on an oscilloscope with an accuracy of 1–3%.

The tests were performed by establishing the airflow at the desired flow rate and total nozzle inlet pressure. This flow of air at room temperature was maintained for about 30 s. Approximately six measurements for each sensor were taken during the following 10 s and were averaged over this period. After the cold flow was established inside the nozzle model, the combustion process with alcohol was initiated. The chamber pressure at nozzle inlet increased suddenly within 0.2 s to the steady-state value for the hot-gas flow, while the temperature measurements on the nozzle outside increased gradually within a few seconds toward a steady-state value. The gradient of this transient temperature rise was evaluated to recalculate the wall heat flux. Wall pressure data were recorded by low-frequency pressure transducers with a measurement uncertainty less than 1% in terms of absolute pressure values.

Figure 13 shows wall pressure profiles in the first cold-gas test runs. The negative pressure gradient contour leads again to a conventional separation characteristic, as observed for the TICNP-nozzle shown in Fig. 9. A corresponding vacuum wall pressure profile from a TDK-flowfield analysis (frozen option) is included for comparison. Figure 14 shows wall pressure and wall heat flux data from two hot-gas test runs. In the first test with $p_c/p_a = 14$, the separation line is attached to the wall inflection; whereas for $p_c/p_a = 16.9$, uncontrolled but stable separation is observed in the nozzle extension. For the latter case, the expected drop in wall heat flux at the wall inflection is quite visible. This shows that the dual-bell nozzle with the characteristic pressure drop at the wall inflection may be used to achieve lower wall heat flux downstream of the wall inflection, as proposed in Ref. 9.

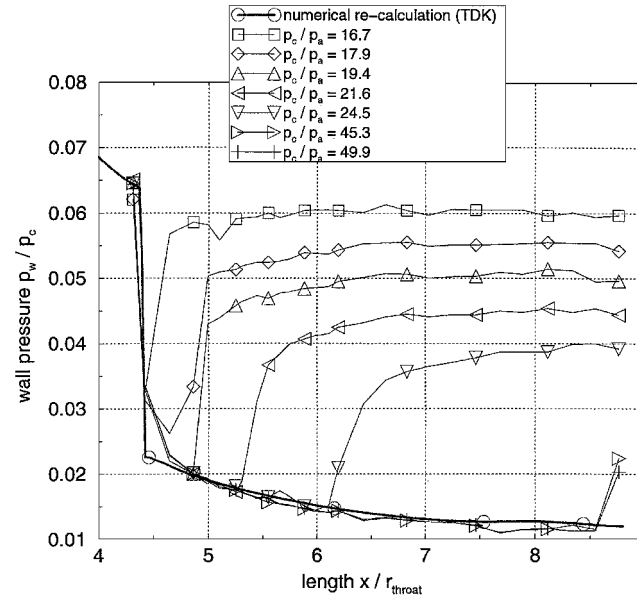

Fig. 13 Wall pressures measured during cold-gas tests with upramping of chamber pressures p_c/p_a in TEHORA dual-bell nozzle.

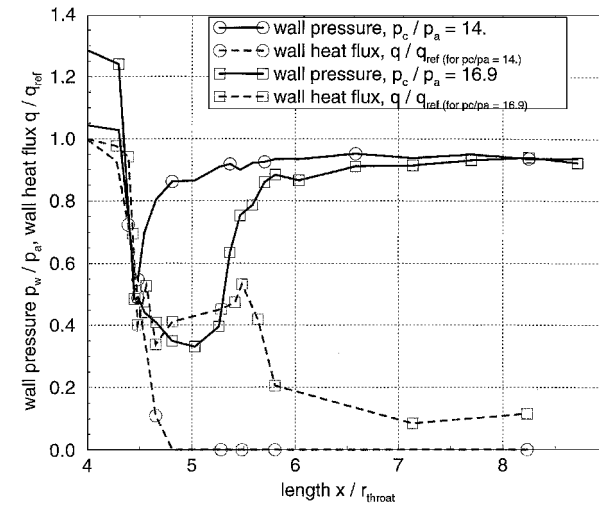

Fig. 14 Wall pressures and wall heat fluxes measured during hot-gas tests with upramping of chamber pressures p_c/p_a in TEHORA dual-bell nozzle.

Furthermore, in the incipient separation region characterized by the steep wall pressure increase from vacuum profile to the plateau value, $5 < x/r_{\text{throat}} < 5.6$, an increase in wall heat flux is observed. In this incipient flow separation region, the flow is still physically attached to the wall.[11–13] The heat flux increase is caused by an increased turbulent mixing and pressure increase due to the boundary-layer/separation-shock interaction. Farther downstream, in the recirculation region with inflow of ambient air, wall heat fluxes decrease again. In this nozzle part, cold ambient air sucked into the nozzle passes the wall, and the observed wall heat flux may be explained due heat conduction inside the nozzle wall and/or due to the radiating freestream shear layer.

The comparison of the separation characteristics of cold- and hot-gas tests reveal slightly higher separation pressures for the hot-gas tests.

Summary

The dual-bell nozzle concept has been investigated by means of analytical and experimental work. Motivated by a former study of the authors, which revealed surprisingly low performance losses due to the wall inflection, a cold- and hot-gas test program was conducted to get insight into the aerodynamic behavior. Special points of interest were the flow transition depending on the nozzle contour design, the time needed for the flow transition, the side loads induced by the transition, and information on the wall heat flux evolution.

From the cold-gas tests with different contour types, it was shown that the analytical design considerations were in very good agreement with test results. Typical timescales needed for the flow transition from sea-level to vacuum operation were less than 10 ms for the constant pressure and overturned pressure contours. For both types of nozzle extensions, a strong hysteresis is observed for the transition pressure ratio, with a higher value for start up. This hysteresis effect actually supports the dual-bell concept because it prevents a potential pulsation between dual-bell operation modes.

Hot-gas tests showed that the pressure drop at the wall inflection significantly reduces the wall heat fluxes farther downstream.

Acknowledgement

The work presented in this paper was partly financed by the German National Program TEKAN and the joint Russian/German Program TEHORA (Förderkennzeichen 50TT9430). Within the frame of TEHORA, the authors acknowledge G. Dumnov, G. Nikulin (Keldysh Research Center), and V. Rubinski (Chemical Automatics Design Bureau) for their cooperation. A part of this work has been performed within the framework of the European flow separation control device working group. The authors acknowledge especially R. Stark (DLR, German Aerospace Research Center), R. Ryden, Th. Damgaard, and J. Östlund (Volvo Aero Corporation), Ph. James (Société Européene de Propulsion), Ph. Reijasse (ONERA), Alziary de Rockefort (University of Poitiers), R. Schwane, and J. Muylaert (ESTEC), M. Pons, P. Vuillermoz, and N. Girard (Centre National d'Etudes Spatiales) for the fruitful cooperation in this field.

References

[1]Foster, C., and Cowles, F., "Experimental Study of Gas-Flow Separation in Overexpanded Exhaust Nozzles for Rocket Motors," Jet Propulsion Lab., Progress Rept. 4-103, California Inst. of Technology, Pasadena, CA, 1949.

[2]Horn, M., and Fisher, S., "Dual-Bell Altitude Compensating Nozzles," NASA-CR-194719, 1994.

[3]Goel, P., and Jensen, R., "Numerical Analysis of the Performance of Altitude Compensating Dual-Bell Nozzle Flows," *7th Annual Symposium*, Vol. 2, NASA Marshall Space Flight Center, 1995.

[4]Kumakawa, A., Tamura, H., Niino, M., Nosaka, M., Yamada, H., Konno, A., and Atsumi, M., "Propulsion Research for Rocket SSTOs at NAL/KRC," AIAA Paper 99-2337, June 1999.

[5]Immich, H., and Caporicci, M., "FESTIP Technology Developments in Liquid Rocket Propulsion for Reusable Launch Vehicles," AIAA Paper 97-3311, July 1997.

[6]Frey, M., and Hagemann, G., "Critical Assessment of Dual-Bell Nozzles," *Journal of Propulsion and Power*, Vol. 15, No. 1, 1999, pp. 137–143.

[7]Zinner, W., Haeseler, D., Mäding, C., Rubinskij, V., Gorochov, V., Chrisanfov, S., and Nikulin, G., "Development of Advanced Technologies for Future Cryogenic Thrust Chamber Applications," AIAA Paper 97-3312, July 1997.

[8]Haidinger, F. A., Görgen, J., and Haeseler, D., "Numerical Prediction of Flow Separation for Advanced Nozzle Concept Applications," AIAA Paper 98-3368, July 1998.

[9]Dumnov, G., Ponomaryov, N. B., and Voinov, A. L., "Dual-Bell Nozzles for Rocket Engines of Launch Vehicle Upper Stages and Orbital Transfer Vehicles," AIAA Paper 97-3089, July 1997.

[10]Frey, M., and Hagemann, G., "Restricted Shock Separation in Rocket Nozzles," *Journal of Propulsion and Power*, Vol. 16, No. 3, 2000, pp. 478–484.

[11]Frey, M., and Hagemann, G., "Flow Separation and Side-Loads in Rocket Nozzles," AIAA Paper 99-2815, June 1999.

[12]Frey, M., Stark, R., and Ciezki, H., "Subscale Nozzle Testing at the P6.2 Test Stand," AIAA Paper 2000-3777, July 2000.

[13]Östlund, J., and Bigert, M., "A Subscale Investigation on Side-Loads In Sea-Level Rocket Nozzles," AIAA Paper 99-2759, June 1999.

[14]Terhardt, M., Hagemann, G., and Frey, M., "Flow Separation and Side-Load Behavior of the Vulcain Engine," AIAA Paper 99-2762, June 1999.

[15]Nickerson, G., Dang, L., and Coats, D., "Two-Dimensional Reference Computer Program," NASA NAS 9-12652, April 1973.

[16]Hagemann, G., Schley, C., Odintsov, E., and Sobatchkine, A., "Nozzle Flowfield Analysis with Particular Regard to Three-Dimensional Plug-Cluster Configurations," AIAA Paper 96-2954, July 1996.